Simulating the hydrological regime of the snow fed and glaciarised Gilgit Basin in the Upper Indus using global precipitation products and a data parsimonious precipitation-runoff model

Nazeer, Aftab; Maskey, Shreedhar; Skaugen, Thomas; McClain, Michael E.

**Important note**
To cite this publication, please use the final published version (if applicable).
Please check the document version above.

# Simulating the hydrological regime of the snow fed and glaciarised Gilgit Basin in the Upper Indus using global precipitation products and a data parsimonious precipitation-runoff model

Aftab Nazeer [a,b,c,*,**], Shreedhar Maskey [b], Thomas Skaugen [d], Michael E. McClain [b,c]

[a] Department of Agricultural Engineering, Bahauddin Zakariya University (BZU), P.O.Box 60800, Multan, Pakistan
[b] IHE Delft, Department of Water Resources and Ecosystems, P.O. Box 3015, 2601 DA Delft, the Netherlands
[c] Department of Water Management, Delft University of Technology, P.O. Box 5048, 2600 GA Delft, the Netherlands
[d] Norwegian Water Resources and Energy Directorate, P.O. Box 5091, Maj. 0301 Oslo, Norway

## HIGHLIGHTS

- The hydrological regime of the Gilgit Basin was analysed using global precipitation data and the precipitation-runoff model.
- The snow cover area and actual ET were simulated using an EB approach and snow cover area was validated with satellite data.
- The contribution of precipitation as rain, precipitation as snow and glacier melt to the river runoff were also analysed.

## GRAPHICAL ABSTRACT
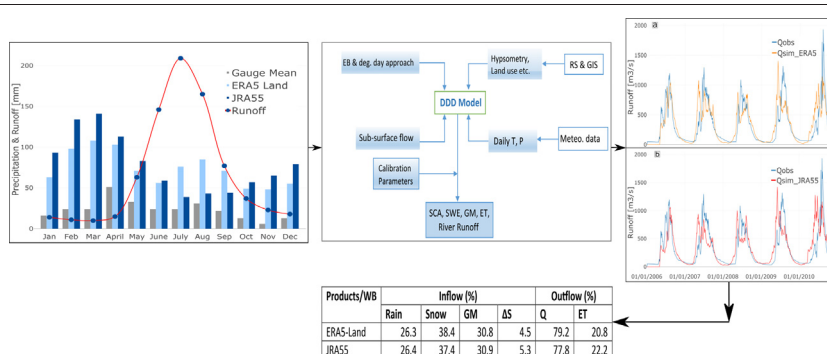
## ABSTRACT

In many high altitude river basins, the hydro-climatic regimes and the spatial and temporal distribution of precipitation are little known, complicating efforts to quantify current and future water availability. Scarce, or non-existent, gauged observations at high altitudes coupled with complex weather systems and orographic effects further prevent a realistic and comprehensive assessment of precipitation. Quantifying the contribution from seasonal snow and glacier melt to the river runoff for a high altitude, melt dependent region is especially difficult. Global scale precipitation products, in combination with precipitation-runoff modelling may provide insights to the hydro-climatic regimes for such data scarce regions. In this study two global precipitation products; the high resolution $(0.1° \times 0.1°)$, newly developed ERA5-Land, and a coarser resolution $(0.55° \times 0.55°)$ JRA-55, are used to simulate snow/glacier melts and runoff for the Gilgit Basin, a sub-basin of the Indus. A hydrological precipitation-runoff model, the Distance Distribution Dynamics (DDD), requires minimum input data and was developed for snow dominated catchments. The mean of total annual precipitation from 1995 to 2010 data was estimated at 888 mm and 951 mm by ERA5-Land and JRA-55, respectively. The daily runoff simulation obtained a Kling Gupta efficiency (KGE) of 0.78 and 0.72 with ERA5-Land and JRA-55 based simulations, respectively. The simulated snow cover area (SCA) was validated using MODIS SCA and the results are quite promising on daily, monthly and annual scales. Our result showed an overall contribution to the river flow as about 26% from rainfall, 37–38% from snow melt, 31% from glacier melt and 5% from soil moisture. These melt

\* Corresponding author at: IHE Delft, Department of Water Resources and Ecosystems, P.O. Box 3015, 2601 DA Delft, the Netherlands.
\*\* Corresponding author at: Department of Agricultural Engineering, Bahauddin Zakariya University (BZU), Multan, Pakistan.
E-mail address: a.nazeer@un-ihe.org (A. Nazeer).

Upper Indus basin
Water balance

simulations are in good agreement with the overall hydro-climatic regimes and seasonality of the area. The proxy energy balance approach in the DDD model, used to estimate snow melt and evapotranspiration, showed robust behaviour and potential for being employed in data poor basins.

## 1. Introduction

Precipitation (P) is the major component in the hydrological cycle but its estimation is the most difficult (Herold et al., 2017). In the Hindukush Karakoram Himalaya (HKH) region, the spatial and temporal distribution of precipitation is largely unknown (Immerzeel et al., 2015). Precipitation can vary enormously over short horizontal distances because of orographic effects and the relation between altitude and precipitation (Bookhagen and Burbank, 2006). The Eastern and South Eastern parts of the HKH region receive summer precipitation due to the Indian monsoon, while the Western part receives most of its precipitation in winter and spring seasons (mostly as snow) under the westerlies effect from the Caspian and Mediterranean seas (Minora et al., 2016). This east to west synoptic scale inconsistency in the precipitation system in the HKH region leads to variations in glacier accumulation (Kaab et al., 2012). Moreover, there is a very low gauge density in the valley floors and virtually no gauges at high altitudes, making rainfall estimates uncertain. Therefore, there is a persistent need to develop and improve the quantification of precipitation at high-altitudes (Immerzeel et al., 2015; Lutz et al., 2014).

In high elevation mountainous watersheds, glacier and snow melt make a significant contribution to flow, which makes them important to the hydrological cycle and downstream water supply, particularly during dry periods (Barnett et al., 2005; Hasson et al., 2014). The largest glaciers of the world after the polar regions (i.e. Arctic circle and Antarctica) are situated in the HKH region (Mukhopadhyay and Khan, 2014a). Water from the HKH region and the neighbouring Tibetan Plateau (TP) are the origin of large river systems such as the Brahmaputra, Ganges, and Indus. Thus, any changes in the glaciers in these mountain ranges may have serious consequences for future availability of water for almost 800 million people residing in these large rivers basins (Mukhopadhyay and Khan, 2014b, 2015).

Quantifying the contributions from seasonal snow and glacier melt to river runoff are challenging but essential for the management and planning of water resources (Schaner et al., 2012). Snow-accumulation measurements with snow pillows and snow pits are also rare and generally limited to short records in the HKH region (Immerzeel et al., 2012). In 1995, the Water and Power Development Authority (WAPDA) of Pakistan installed snow pillows at various sites on the Pakistan side of the HKH region in a joint venture with a Canadian team (SIHP: Snow and Ice Hydrology, 1997). However, many of the installed pillows faced transmission system issues and unexpected "jumps" associated with ruptures and ice bridging effects. The remotely sensed data coupled with a geographical information system (GIS) has proved a powerful tool for mapping glaciers and snow covers in inaccessible and rugged terrains (Tong et al., 2009). However, these snow and glacier monitoring techniques by remote sensing data are subject to various limitations and biases, including cloud coverage, dense vegetation, surface heterogeneity, low resolution and spectral similarities (Berthier et al., 2006). Consequently, the current understanding of snow and glacier cover status and their contribution to the river runoff is poor and based on insufficient analysis with very limited data. So increased measurement of ongoing accumulation and melt rates for snow and glaciers is needed to estimate future regional water resources availability (Barnett et al., 2005).

Recent studies by (Cannon et al., 2015) in the HKH region indicate a strong and enhanced frequency of winter westerlies (1979–2010), and consequently increased winter precipitation. Kapnick et al. (2014) concluded that the Karakoram snow fall is not reduced due to climatic

warming as the seasonal snowfall cycle is subjected to the westerlies instead of monsoon winter precipitation. Michaelides et al. (2009) noted that there are four principal methods to estimate precipitation: (1) ground-based gauges (2) ground-based radar (3) satellite based remote sensing (4) atmospheric reanalysis products. The ground based gauges have a problem of gauge density and cannot reflect the true rainfall variability and thus result in inaccurate assessments of areal rainfall (Andréassian et al., 2001). The ground based radars have higher spatio-temporal resolution but have limited coverage and are thus restricted to regional scale estimates (Martens et al., 2013). Satellites can observe large areas with high spatio-temporal resolution compared to radar (Smith, 2006) but satellite based estimates are vulnerable to systematic biases, unable to detect low intensity rainfall, and perform poorly over surfaces covered with snow and ice (Mugnai et al., 2013). Reanalysis products are suitable for describing large-scale weather systems, but tend to fail on the variability because of their low spatio-temporal resolution (Kidd et al., 2013). These products can, however, potentially provide precipitation estimates in data scarce regions, assist to fill gaps in data, and ultimately support a better understanding of the hydrology (Shafeeque et al., 2019).

Hydrological models vary in process representation, applications and spatial scale ranging from small catchments to global scale (Skaugen et al., 2018). For snowmelt estimation, there are two basic modelling approaches i.e. the energy balance and the temperature index (Prasad and Roy, 2005). Several snowmelt estimating models have been designed for specific needs and various hydrologic conditions. Some of these models are very intensive regarding input data and/or complicated to setup and operate. Only a few models can handle difficult hydrologic conditions (Tekeli et al., 2005) like in the HKH region with its very high altitude, complex topography and weather system. Investigating snow and glacier conditions in data poor basins and with a changing climate requires models that: (1) are efficient in terms of running at varying spatial and temporal scales; (2) are parsimonious in terms of input data; and (3) have physical and identifiable model parameters (Skaugen et al., 2018). Many snow model inter comparison projects have been launched in the last decades for different aims with common conclusions including: (1) there is no 'best' snow model and; (2) complexity in model structure does not necessarily mean improved performance (Essery et al., 2013).

The economy of the Indus region largely depends upon irrigated agriculture, and irrigation systems in the region are highly depend on melt water (Akhtar et al., 2008). There is an increasing food demand in line with a remarkable growth of population in the Indo-Gangetic plain. Almost 70% of the total flow in the River Indus is generated by seasonal snow and glacier melt from the UIB (Mukhopadhyay and Khan, 2015; SIHP: Snow and Ice Hydrology, 1997). The Indus Basin Irrigation System (IBIS) is the largest irrigation system world-wide, irrigating 17 million hectares (M ha) of a total 24 M ha of cultivable area in Pakistan (Akhtar et al., 2008; Khan et al., 2014).

The primary analysis of observed hydro-meteorological data of Gilgit River (one of the main tributaries of Indus) shows an annual average runoff of about 743 mm for the 1995–2010 period. But the basin-averaged annual precipitation derived by the arithmetic mean of the data from four installed stations in the Gilgit Basin shows 277 mm for the same period. During the hydrological model's calibration and validation frameworks, this underestimated precipitation is often compensated through sub-optimal adjustment of the model's parameters (for example evapotranspiration, soil properties, melt factors, etc.) (Lutz et al., 2014). These calibrated parameters can hence induce

uncertainties and biases for flow dynamics. Few modelling based investigations (Adnan et al., 2017; Latif et al., 2020; Tahir et al., 2016) were carried for the Gilgit Basin and all of these used a temperature index approach. In snow fed and glaciated basins, the temperature-index based hydrological models often inadequately represent the prevailing energy balance and may not accurately simulate hydrologic processes (Dahri et al., 2021). To derive and understand the hydrological processes, especially for glaciated and snow covered basins with little or no observations, we see a need for more realistic and spatially distributed precipitation estimates. Hence our analysis is novel in four ways; i) in our model, the snowmelt and evapotranspiration are simulated using the energy balance approach, not using calibrated temperature index models, ii) the parameter parsimony of our model makes it more realistic where, unlike other modelling approaches, the flow dynamics are derived partly from catchment characteristics using GIS, iii) we also took advantage of more recent global precipitation datasets, for example, ERA5-Land and the satellite datasets, for example, Randolph glacier inventory (RGI) version 6.0 and LandSat-8 and iv) we have assessed the performance of our model using the Kling Gupta efficiency (KGE) that describes correlation, errors in variability and bias and addresses several apparent shortcomings in Nash–Sutcliffe Efficiency (NSE). In addition, we have also attempted to quantify the different flow components and the water balance for the Gilgit Basin. The overarching objective for this study is to improve the current understanding of hydrological regime of the snow fed and glaciated Gilgit Basin using precipitation-runoff modelling and global precipitation products. To derive and understand the hydrological processes for a glaciated and snow covered basin with little or no observations, we see a need for more realistic and spatially distributed precipitation estimates using more recent global data sets. In addition, we believe that by applying a comparatively newly developed modelling approach (semi-distributed, parameter-parsimonious and developed for different parts of the world but similarly snow/glacier dominated basins), this study complements the previous modelling studies to enhance our understanding of the basin's hydrological regime. The outcomes of this study include improved precipitation estimates, enhanced understanding of the flow regime, snow covered area (SCA), snow water equivalent (SWE) and glacier melt (GM). The study also includes the SCA validation against the satellite data and assesses the consistency of the snow water equivalent and glacier melt with the hydro-climatic regime of the region.

## 2. Study area

The Gilgit Basin, one of the sub-basins of the UIB, in the Hindu Kush mountainous region, was selected for this study. The basin lies between the longitudes of 35°46′05″ to 36°1′16″ N and latitudes of 72°25′02″ to 74°19′25″ E with an area of 12,726 km$^2$ as derived from the Shuttle Radar Topography Mission (SRTM) 30 m digital elevation model (DEM). The elevation of the basin varies from 1454 to 7151 m above sea level (masl) with a mean elevation of 4054 masl. The Randolph glacier Inventory (RGI 6.0) (Muhammad et al., 2019), showed that the basin has a glacier cover of about 8.1% (1030 km$^2$) with more than 75% above an elevation of 4500 masl (Fig. 1). The seasonal snow cover varies from 95% in winter to 5% in summer (Adnan et al., 2017; Hasson et al., 2014). The elevation gradient in Gilgit Basin is very steep and about 70% of the area lies between 3500 and 4900 masl (Table 1). Gilgit River starts from Shandoor Lake at an elevation of about 3738 masl. The seasons of this region are generally divided into four; winter season (Dec, Jan, Feb); spring season (March, April, May); monsoon season (June, July, August, September) and post monsoon season (October, November). The river network in this basin consists of a few main tributaries like the Yasin, Phandar, and Ishkoman. The river flows in a North West to South East direction, passes through Gilgit City, and joins River Hunza at Alam Bridge and finally joins the river Indus. Gilgit River has an annual mean runoff measured at Gilgit Bridge gauging station from 50 years of record (1961–2010) of 288.6 m$^3$/s.

However, hydrological modelling based quantitative evaluation of the contributions of melt water from seasonal and perennial snows and glaciers are rarely available.

As the climatic variables are strongly influenced by altitude, the altitudinal variation of about 6000 m gives Gilgit Basin a complex climate (Sharif et al., 2013). The valley floors of the basin are arid with annual rainfall ranging from 100 to 200 mm, but at higher elevation, precipitation increases (Cramer and Leemans, 1993). The climate of the basin is a result of the complex interaction among monsoon circulation, westerlies effects and the local topography. The monsoon is the primary and largest source of precipitation in the Himalayan range, but this influence decreases moving in a north-western direction, and mid-latitude westerlies become the primary source of precipitation (Lutz et al., 2016). The Hindukush range receives precipitation from both of these sources and gives the basin two main periods of maximum precipitation; the winter/spring period from December to April (i.e. the westerlies influenced period) and the summer period July through September (i.e. the monsoon influenced period) (Bocchiola et al., 2011). The mean monthly temperatures in areas above 3000 masl, influenced by the westerlies, remain below the freezing point between October and March. There is hence no direct flow during this period (Archer and Fowler, 2004). For this low flow period, runoff is mainly due to the precipitation from lower altitudes and groundwater discharge (Hasson, 2016). For summer, the runoff from higher elevations is primarily due to seasonal snow and glacier melt. The Gilgit Basin hosts four metrological stations (Gilgit, Gupis, Yasin and Ushkore) at elevation ranges from 1460 to 3353 masl. The Gilgit and Gupis stations are at low altitude and have long records available from 1951 to the present. While the high altitude Ushkore and Yasin stations records are available from 1995 to present.

## 3. Datasets & methodology

### 3.1. Meteorological data

The meteorological data for Gilgit Basin were obtained for four stations in the basin from the Pakistan Metrological Department (PMD) and Water and Power Development Authority (WAPDA), federal level departments of Pakistan. Two of these stations; Gilgit (1460 masl) and Gupis (2156 masl) were installed by PMD and the remaining two; Yasin (3353 masl) and Ushkore (3353 masl) by WAPDA (Table S1). These data are freely available for research purposes. PMD records meteorological data are at relatively low altitudes from 1952 to present. WAPDA records hydro-meteorological data, with stations at comparatively high altitudes, but for a relatively short period. These stations have monthly maximum precipitation in the month of April and minimum in November, while the seasonal data have maximum precipitation in winter/spring season and minimum in the autumn/early winter. From the 1995–2010 records, the Gilgit station has the minimum precipitation and Ushkore station the maximum. The mean annual precipitation, recorded from to 1952–2008, is 135 mm and 185 mm for Gilgit and Gupis stations, respectively (Tahir et al., 2016), while the mean annual precipitation recorded from to 2002–2010 data is 367 mm for both Yasin and Ushkore stations (Fig. S1). All these records, however, contain missing data varying from a single day to a full year.

The annual average temperature at Gilgit, Gupis and Ushkore climatic stations was 15.99 °C, 12.8 °C and 6.02 °C, respectively, for the 1995–2010 period. Monthly mean figures show that maximum temperature was recorded in July and minimum in January for all stations (Fig. S2). There is clear daily variability in temperature that ultimately affects all hydrological processes related to temperature.

### 3.2. Runoff data

The Gilgit River has a gauging station installed at Gilgit Bridge at an elevation of 1454 masl. Daily runoff data are recorded and maintained
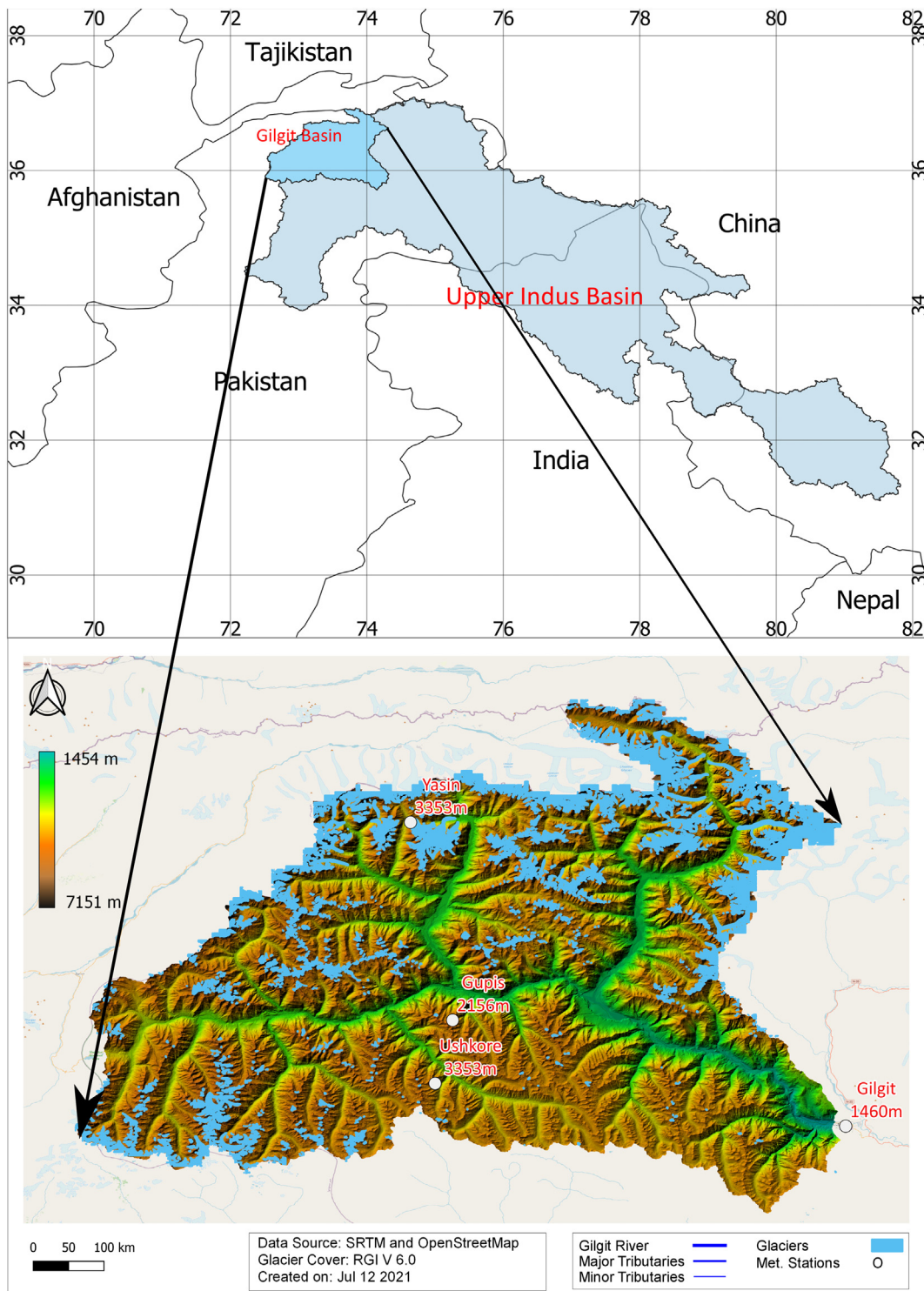
**Fig. 1.** Location of study Area with Digital Elevation Model (DEM), glacier cover, river network and meteorological stations.

by WAPDA with a period of record running from 1966 to present. According to hydrological regimes defined by Krasovskaia et al. (1994), the observed runoff shows two major flow regimes. One is the low flow regime or the base flow from October to March. The main source of this flow is liquid precipitation and groundwater discharge. The second is the high flow regime from April and to September. This high flow regime is further divided into two regimes: one is snowmelt dominated from April to mid/late June and second is glacial melt dominated from late June to the end of September (Hasson, 2016; Mukhopadhyay and Khan, 2014a). Similar to other high

elevation basins in the HKH region, melt contribution is significant in the Gilgit Basin. Runoff data from 1995 to 2010 were used in this study.

### 3.3. Precipitation from global datasets

Many global products have been developed and are freely available with varying data sources, temporal coverage, temporal resolution, spatial coverage and spatial resolution. The following two products are selected for this study.

**Table 1**
Hypsometry of the Gilgit Basin (divided into 10 elevation bands of equal area) and glacier cover (Source: Shuttle Radar Topography Mission Digital Elevation Model, DEM, 30 m; & Randolph glacier Inventory, RGI 6.0).

| Area | Area quantiles | Elevation range (m) | Mean elev. (m) | Glacier cover (%) |
|------|------|------|------|------|
| a1 | 10 | 1454–2916 | 2185 | 0 |
| a2 | 20 | 2917–3441 | 3178 | 1 |
| a3 | 30 | 3442–3772 | 3606 | 2 |
| a4 | 40 | 3773–4019 | 3895 | 3 |
| a5 | 50 | 4020–4213 | 4116 | 3 |
| a6 | 60 | 4214–4369 | 4219 | 4 |
| a7 | 70 | 4370–4515 | 4442 | 6 |
| a8 | 80 | 4516–4677 | 4596 | 11 |
| a9 | 90 | 4678–4899 | 4788 | 19 |
| a10 | 100 | 4900–7151 | 6025 | 32 |

### 3.3.1. ERA5-Land

The European reanalysis 5 (ERA5) Land is a newly developed data set available for the period from 1981 to present with 2–3 months delays. ERA5-Land data have 0.1° degree spatial resolution and hourly temporal resolution and were acquired freely from https://cds.climate.copernicus.eu/. The temporal and spatial resolutions of ERA5-Land are high and make it very useful for all kinds of land surface applications such as flood or drought forecasting. The model used in the production of ERA5-Land is the tiled European Centre for Medium-Range Weather Forecasts (ECMWF) Scheme for Surface Exchanges over Land incorporating land surface hydrology (H-TESSEL). The data are produced under a single simulation, without coupling to the atmospheric module of the ECMWF's Integrated Forecasting System (IFS) or to the ocean wave model of the IFS. It runs without data assimilation, making it computationally affordable for relatively quick updates (Muñoz Sabater, 2019). ERA5-Land is selected for this study because it is the latest published data from ECMWF and has a fine spatial resolution.

### 3.3.2. JRA-55

The Japanese reanalysis (JRA-55) data set is the non-gauge corrected, third-generation reanalysis spanning from 1958 to present with several days delay. The data have 0.56° spatial resolution and 3-hourly temporal resolution and were acquired freely from http://jra.kishou.go.jp/JRA-55/. Compared to the previous generation reanalysis data sets of Japanese Meteorological Agency (JMA), JRA-25, JRA-55 uses a further advanced data assimilation scheme, several new observational data sources, increased model resolution and a new bias correction technique for satellite data (Kobayashi et al., 2015). JRA-55 is selected for this study due to its documented performance in literature and from an initial analysis where it showed reasonable precipitation estimates for our case study.

### 3.4. Satellite based data

The satellite based data used in this research includes the Shuttle Radar Topography Mission (SRTM) 30 m DEM, the Randolph Glacier Inventory (RGI 6.0), land cover data from LandSat-8 and Moderate Resolution Imaging Spectroradiometer (MODIS) satellite data. SRTM data are generated by the U.S. National Aeronautics and Space Administration (NASA) and are accessed freely from their official website. These data were used for catchment delineation, area elevation information, river network and to derive model parameters for the precipitation-runoff model. The RGI is an initiative by *Global Land Ice Measurements from Space* (*GLIMS*) to monitor the world's glaciers using optical satellites. The RGI data are accessed from GLIMS database and are used to derive glacier cover in elevation zones in the Gilgit Basin (Fig. 1). LandSat-8 data are the most recent data by the Landsat Data Continuity Mission (LDCM) with 30 m spatial and 16 days temporal resolution. The MODIS snow and ice data were accessed from published data (Hussan et al., 2020) for Gilgit Basin and used for validating the SCA simulations by the precipitation-runoff model.

### 3.5. Runoff modelling

#### 3.5.1. Distance Distribution Dynamics (DDD) hydrological model

The Distance Distribution Dynamics (DDD) model is a conceptual, semi-distributed, catchment based precipitation-runoff model, scripted in R and Julia programming that can simulate runoff at daily or even smaller time steps (Skaugen and Onof, 2014). The model was developed by the Norwegian Water Resources and Energy Directorate (NVE) and is used at the Norwegian flood forecasting service. The main aim for developing this model was to keep the number of parameters requiring calibration at a minimum, while maintaining the precision and required detail of the simulations (Skaugen et al., 2018). Moreover, a majority of model parameters are derived from observed data and not calibrated against runoff (Skaugen and Weltzien, 2016). The model requires temperature and precipitation input values for all zones. The model simulates runoff for a given catchment, accumulation, melt and distribution of snow, glacier melt, actual evapotranspiration (ET) and saturated and unsaturated soil water (Skaugen and Weltzien, 2016). Snowmelt and evapotranspiration are calculated using an energy-balance (EB) approach. The EB approach consists of proxy models and is driven entirely by precipitation and temperature data. The EB based parameters are calculated using geographical location, Julian day information (for short wave), and algorithms used in Skaugen and Saloranta (2015) and Walter et al. (2005) for energy-balance modelling. The following is the main EB equation used in the DDD model;

$$M = (S_w + L_a - L_t + H + LE + G + R - CC) \times \left(\frac{1}{\lambda_F \times \rho_w}\right) \qquad (1)$$

where;

M: change in the snow water equivalent in mm,
$S_w$: net short wave radiation in $KJm^{-2}$, $L_a$: atmospheric long wave radiation in $KJm^{-2}$,
$L_t$: terrestrial long wave radiation in $KJm^{-2}$, H: sensible heat exchange in $KJm^{-2}$,
LE: energy flux in $KJm^{-2}$ (the latent heat of vaporization), G: ground heat conduction in $KJm^{-2}$,
R: heat added due to precipitation in $KJm^{-2}$, CC: change in snowpack heat in $KJm^{-2}$,
$\lambda_F$: 335 $KJKg^{-1}$ (latent heat of fusion) and, $\rho_w$: 1000 $kgm^{-3}$ (density of water).

In the subsurface module, the capacity of the subsurface water reservoir is shared between a saturated groundwater zone and an unsaturated soil water zone (Skaugen and Mengistu, 2016). The subsurface variables are updated after evaluating if the current soil moisture together with the precipitation input (rain and snowmelt) represent an excess of water over the field capacity, which is fixed at 30% (Skaugen and Onof, 2014). If so, the excess water is added to the saturated zone.

#### 3.5.2. Setting up the DDD model

GIS analysis was performed using the SRTM 30 m DEM, RGI and LandSat-8 data. The catchment was divided into 10 elevation zones of equal areas as this is the requirement of the model. The LandSat-8 for land cover and SRTM 30 m DEM are used to derive the distances from the points in the catchment to the nearest river for bogs and soil parts of the catchment. These datasets are also used to derive the fractions of land use classes in the catchment (for example soils and bogs) and the river network. The fraction of glacier area present in all sub areas is derived from RGI 6.0. The basin area is delineated and divided into 10 sub area/zones of equal size and mean elevation is derived for all zones (Fig. S3). The runoff dynamics (for example distances for river network) are derived entirely from catchment characteristics using GIS and recession analysis of runoff (Skaugen and Mengistu, 2016). The spatial distribution of snow is parameterized using spatial

variability in observed precipitation, following (Skaugen and Weltzien, 2016), in which the shape parameter of gamma distributed unit snow ($a_0$) and decorrelation length (D) are derived from the relationship between the spatial mean and spatial variance of positive precipitation (excluding zeros). The temperature is calculated for each elevation zone applying temperature lapse rate on Ushkore station (3353 masl) data. To derive the lapse rate, first the lapse rate existing among all stations located at different elevations was derived using Eq. (2). Then a simple arithmetic mean was calculated to get one weighted value for daily interval of n.

$$TLR = (T_i\_T_j)/(Z_i\_Z_j) \tag{2}$$

TLR is the temperature lapse rate, $T_i$ and $T_j$ are temperature at gauges and $Z_i$ and $Z_j$ are elevations of gauges, respectively.

The precipitation data were derived for the whole catchment from ERA5-Land and JRA-55 and were further derived for all 10 elevation zones. The precipitation data sets are analysed using command line suite based Climate Data Operators (CDO). The study area is covered with more than 130 grid cells of ERA5-Land and 12 grid cells of JRA-55 data. To facilitate the data extraction for each elevation zone and to capture the northeast part of the study area well, a higher resolution grid

size is needed. Both data sets were resampled from their actual resolution to a common resolution of 1 km² applying the nearest neighbour algorithm. The DDD model also needs to calibrate some parameters. Table S2 shows these parameters with the calibration ranges and values used for the current simulations for both datasets. Table S3 shows parameters calculated using GIS analysis, recession analysis and fixed values.

### 3.5.3. Performance evaluation

For accuracy assessment the skill scores of Kling Gupta efficiency (KGE) and bias (%) were used. The KGE (Eq. (3)) is the goodness-of-fit measure developed by Gupta et al. (2009). KGE describes correlation and errors in variability and bias and addresses several apparent short-comings in Nash–Sutcliffe Efficiency (NSE) (Knoben et al., 2019). It is increasingly used for model calibration and evaluation with value ranges from minus infinity to 1.

$$KGE = 1 - \sqrt{(r-1)^2 + \left(\frac{\sigma sim}{\sigma obs} - 1\right)^2 + \left(\frac{\mu sim}{\mu obs} - 1\right)^2} \tag{3}$$

where; r is the linear correlation between observations and simulations, $\sigma sim$ and $\sigma obs$ are the standard deviations of simulations and
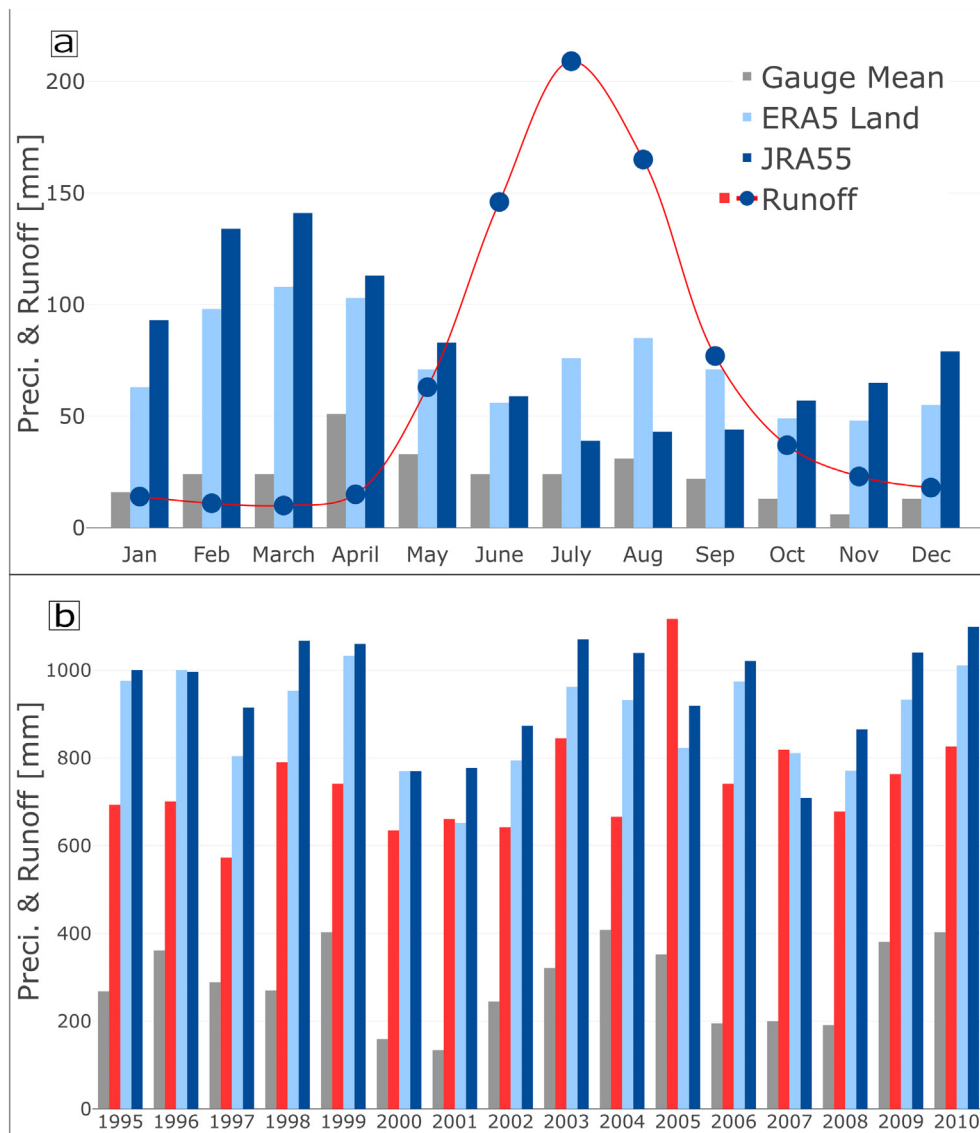


Fig. 2. Mean a) monthly and b) annual precipitation from European reanalysis 5 (ERA5-Land), Japanese reanalysis (JRA-55) and basin-averaged station data vs runoff from 1995 to 2010.

observations, respectively, and *μsim* and *μobs* are the means of simulations and observation, respectively.

## 4. Results and discussion

### 4.1. Climatology of temperature

The highest elevation zone is located at 6025 masl, whereas the highest temperature gauge is at 3353 masl. In order to derive the mean temperature for all zones, a temperature lapse rate was applied considering the Ushkore station (3353 masl) data as reference. The variation in temperature derived for all zones is high due to the high variation in gauged data. The weighted lapse rate values for all days of the 1995–2010 period were obtained using Eq. (2). Daily lapse rate (DLR) varied highly from a maximum of $-11.48$ °C km$^{-1}$ to $-3.83$ °C km$^{-1}$. Lapse rates were also calculated for the whole catchment for the whole period (a fixed lapse rate) as well as on a monthly and seasonal basis. The fixed lapse rate (FLR) for the whole time series is estimated as $-5.74$ °C km$^{-1}$. For monthly lapse rate (MLR), twelve mean values were derived for all months showing maximum lapse rate of $-7.04$ °C km$^{-1}$ for the month of March and minimum values as -—.81 °C km$^{-1}$ for the month of September. The seasonal lapse rate (SLR) determined as $-6.09$ °C km$^{-1}$, $-6.65$ °C km$^{-1}$, $-5.03$ °C km$^{-1}$ and $-5.28$ °C km$^{-1}$ for winter, spring, monsoon and post-monsoon seasons, respectively. After comparing these options, SLR was used to derive temperature of all zones for this study because it induces least variations in derived temperature for all elevation zones.

### 4.2. Climatology of precipitation

The precipitation for Gilgit Basin is derived from the coarse resolution ($0.55° \times 0.55°$) re-analysis data set JRA-55 and the high resolution ($0.1° \times 0.1°$) data set ERA5-Land. The daily estimates are quite reasonable for both data sets except that the JRA-55 data have more wet days compared to the ERA5-Land data. The maximum daily basin mean precipitation in ERA5-Land is 59 mm (on 27 August 1997) and in JRA-55 is 37 mm (on 25 April 2003). Both global datasets have more rainy days in the study area compared to the gauged data. The monthly and annual mean (Fig. 2) precipitation estimates from global data sets showed improvement in both quantification and temporal variability when compared to runoff than gauged precipitation. The variability in mean monthly precipitation is higher for JRA-55 with a maximum of 141 mm for March and minimum of 39 mm in July compared with ERA5-Land, which showed a maximum of 108 mm in March and a minimum of 48 mm in November.

The ERA5-Land data indicate the study area receives 25% of its precipitation during winter, 32% during spring, 32% during monsoon and 11% during post monsoon season. The JRA-55 data indicate this proportion to be 32% during winter, 36% during spring, 19% during monsoon and 13% during post monsoon season. As the study area is dominated by westerlies precipitation, both products are in line in capturing the spring precipitation. The basin also receives significant monsoon summer precipitation that generates river flow. The comparison of grid precipitation with that where stations are located shows JRA-55 performs poorly in observing the monsoon precipitation. However, the ERA5-Land data behave very well in regards to the monsoon precipitation which might be due to its high spatial resolution. The gauged data showed that the basin has minimum precipitation in the post monsoon season (Oct–Nov) and both dataset capture this. The seasonal trends of maximum precipitation in spring and minimum in post monsoon showed by both data sets are also evident from station data especially for the spring period. The ERA5-Land data showed an annual mean precipitation of 888 mm and JRA-55 951 mm, from 1995 to 2010 data. The ERA5-Land data had maximum rainfall in 1999 followed by 2010 and JRA-55 in 2010 followed by 2003. While the minimum rainfall recorded by both ERA5-Land and JRA-55 was in the years 2000 and 2001. Overall,

both data sets are reasonably good for capturing the maximum and minimum precipitation.

#### 4.2.1. Altitudinal variation of precipitation

The altitudinal analysis of the precipitation estimates from the global data sets revealed unusual characteristics in the study area. The lowest elevation zone showed the maximum annual precipitation while the highest elevation zone receives the least annual precipitation for both data sets (Fig. 3a). This zonal based analysis shows a negative precipitation gradient in the three lowest zones of the basin (1454 to 3772 masl), a slight positive gradient from the fourth to seventh zones (3773 to 4515 masl) and a negative gradient for the remaining three highest zones (4516 to 7151 masl). The seasonal precipitation also shows a slight negative gradient for both JRA-55 based (Fig. 3b) and ERA5-Land based estimates (Fig. 3c).

### 4.3. Runoff simulations

The precipitation-runoff model is set up for the Gilgit Basin to improve our understanding of the hydrological regime, and in particular, the snow and glacier melts. The model is driven by global precipitation data (JRA-55 & ER5-Land) and gauged based temperature data as main inputs. The SRTM DEM based topography and river network, LandSat-8 based land cover data, and RGI 6.0 based glacier cover data were also used to estimate model parameters and determine catchment characteristics. The over- and/or under-estimation of precipitation by the global products is corrected by applying rain and snow correction factors (Pkorr and Skorr) in the model. The satellite derived snow cover data were used to validate the simulated snow cover area. The model was calibrated Fig. S4 on daily flow from 1995 to 2004 and validated Fig. 4 on 2006–2010 data. To evaluate the performance of the model in the calibration and validation periods, the efficiency criteria of KGE was used. The model performs satisfactorily in calibration and validation mode using both precipitation products as input to the model. The simulated runoff by the DDD model using ERA5-Land and JRA-55 as precipitation input (respectively), matches reasonably well with the observed flow. Simulations showed promising results for the study area with a slightly better performance using ERA5-Land data. The simulations based on ERA5-Land achieved a maximum KGE of 0.76 and 0.78 whereas the JRA-55 based simulation achieved 0.70 and 0.72 for calibration and validation, respectively. The DDD model also simulates the actual evapotranspiration based on the Priestley-Taylor equation, which is quite similar but simplified compared to the Penman-Monteith equation. The annual mean actual evapotranspiration is 203 mm for ERA5-Land based and 221 mm for JRA-55 based simulations. The simulated flows have two peaks, one in early summer possibly due to the snowmelt contributions and second in late summer due to the glacier melt. As snow or glacial melt curves are normally gradually changing so the late summer flow peak may be a combination of monsoon and glacier melt where monsoon causes short term variations in peaks. The simulated flow recession is in good agreement with the observed recession for the whole period. The high peaks of observed flow were not simulated well by the model, however, ERA5-Land data performed slightly better in this regard.

### 4.4. Snow cover area simulations and validation

To simulate the snow in each elevation zone, the model uses a temperature threshold to decide whether the precipitation is snow or rain. Fig. 5a shows how the snow starts melting in March, has a minimum in August and starts accumulating in September. The simulations showed JRA-55 has a slightly higher SCA and more intense snow events due to overestimation of precipitation compared with ERA5-Land. These simulations are validated with MODIS satellite derived daily SCA from published data (Hussan et al., 2020) for the Gilgit Basin for 2006–2010 (Fig. 5a). The ablation and accumulation timing of simulated SCA also
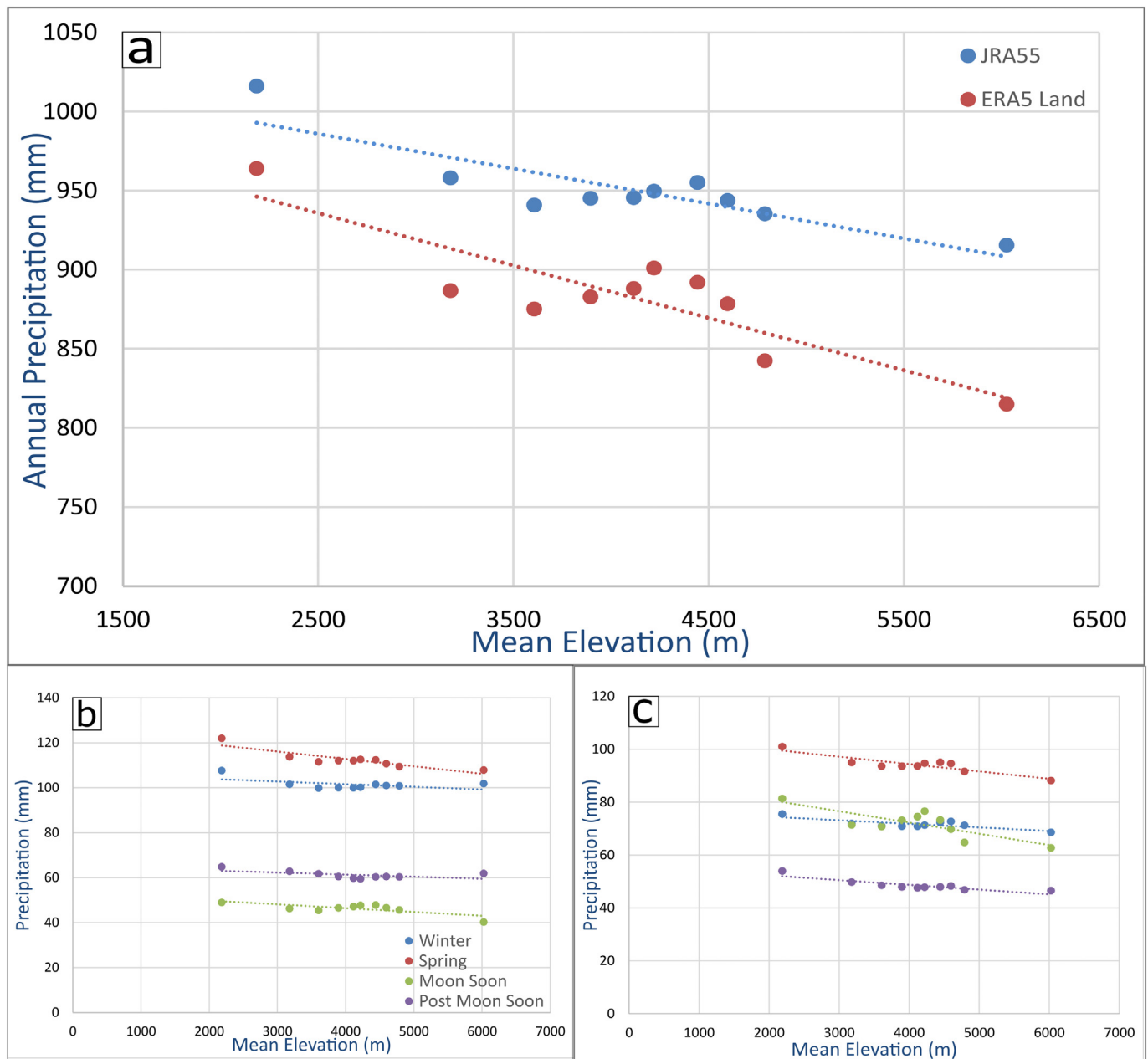
**Fig. 3.** Altitudinal variation of a) annual and seasonal b) Japanese reanalysis (JRA-55) and c) European reanalysis 5 (ERA5-Land) based precipitation for 10 elevation zones of the Gilgit Basin.

seems in good agreement with satellite derived SCA. The sudden rise or drop of temperature in winter or summer season, respectively, generates very short and abrupt snowmelt or snow accumulations. That ultimately causes sudden changes in snow cover which are evident from the both; MODIS SCA and model based SCA. The monthly mean estimates for SCA from DDD and MODIS are in good agreement except that DDD derived SCA has a slightly higher SCA than the MODIS during winter months. The DDD simulated the maximum monthly mean snow cover for January as 97% for both data sets while the MODIS has its maximum in February as 87%. The minimum monthly mean snow cover by all products was 5% by DDD model and 13% by MODIS data. However, the model simulated SCA for the early summer months (May–July) are a bit lower than the MODIS SCA. The annual mean snow cover (Table 2) simulated by DDD model was 55.3% by ERA5-Land, 55.6% by JRA-55 and 57.5% by MODIS data. The higher values by the MODIS data may be because MODIS considers glacier cover also as snow.

*4.5. SWE simulations*

Fig. 5b shows the time series of SWE simulated by the DDD model using JRA-55 and ERA5-Land as input to the model. The SWE increases in October and peaks in February. With the rise in temperature in March, snowmelt starts contributing significantly to the river runoff and becomes less significant with the start of glacier melt but continues melting until the winter starts in October. Similar to SCA, the SWE based on JRA-55 data is slightly higher than ERA5-Land based estimates. The SWE varies highly due to variability in temperature. The model simulated the maximum monthly mean SWE in February as 336 mm using ERA5-Land and 360 mm using JRA-55. Maximum SWE is simulated for 2009 as 382 mm by ERA5-Land and 376 mm using JRA-55, while minimum SWE is for 2007, 272 mm and 241 mm by ERA5-Land and JRA-55, respectively. The annual mean (Table 2) simulated SWE is 316 mm and 312 mm by ERA5-Land and JRA-55, respectively.
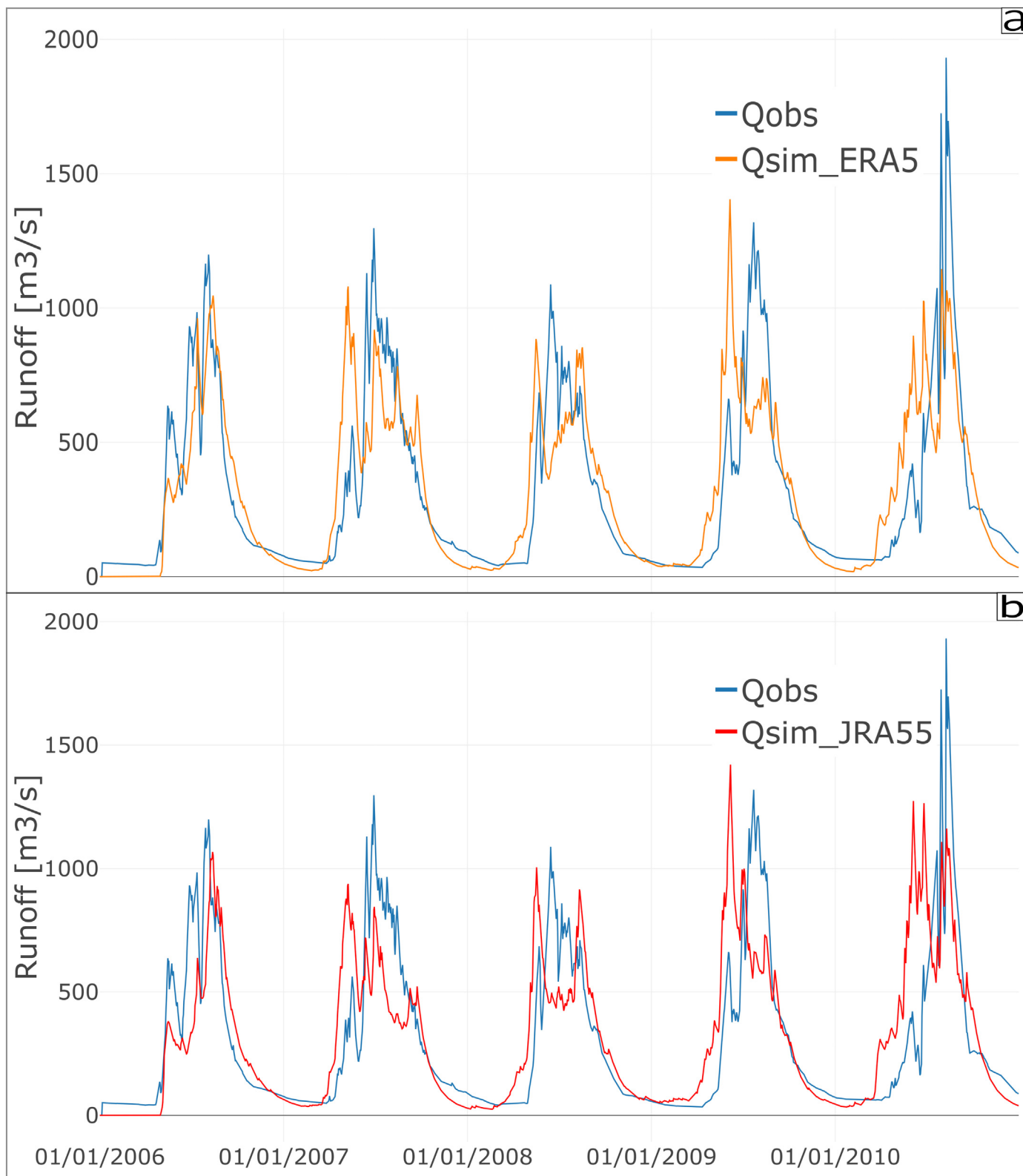
**Fig. 4.** Observed runoff vs simulated runoff by model for validation period (2006–2010) using a) European reanalysis 5 (ERA5-Land) and b) Japanese reanalysis (JRA-55) as input.

### 4.6. Glacier melt simulations

The glacier melt from the study area is calculated using a degree day approach, built as a subroutine in the DDD model. The study area has 8.1% glacier coverage (RGI 6.0) between elevations of 3000 m to 7151 m with more than 75% of glacier cover at an elevation of more than 4500 m. The day to day glacier melt varies greatly mainly because of variation in temperature. The simulated glacier melt based on both data sets indicates melt matches well with the flow regime (Fig. 5c). The glaciers begin melting in early summer (end of April) at low altitude
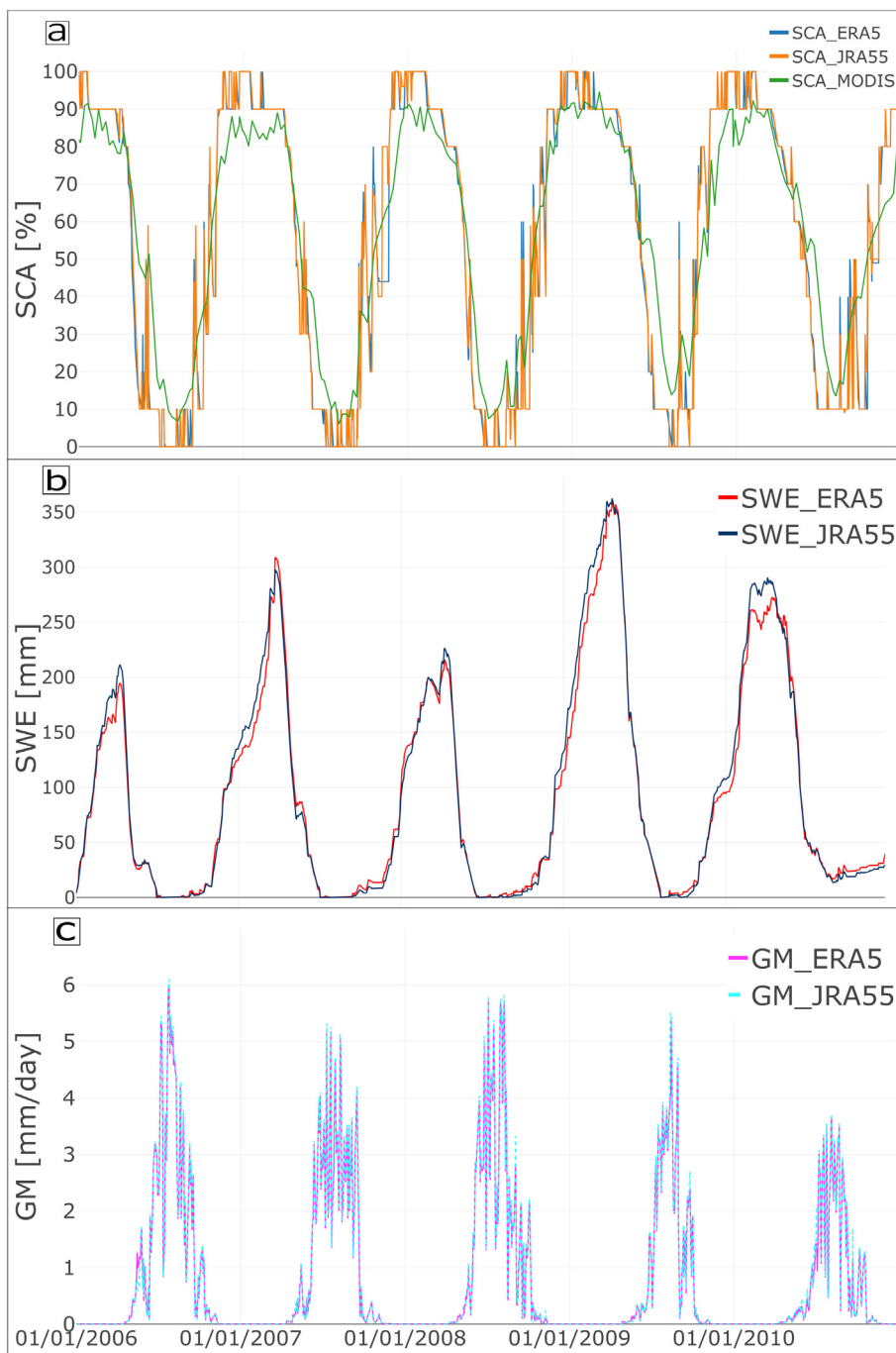
**Fig. 5.** Basin scale time series of simulated a) snow cover area (SCA) vs Moderate Resolution Imaging Spectroradiometer (MODIS) SCA, b) snow water equivalent (SWE) and c) glacier melt (GM).

**Table 2**
Annual mean snow cover area (SCA), snow water equivalent (SWE) and glacier melt (GM) by model and SCA by Moderate Resolution Imaging Spectroradiometer (MODIS).

| Year/results | SCA (%) | | | SWE (mm) | | GM (mm) | |
|---|---|---|---|---|---|---|---|
| | ERA5 | JRA-55 | MODIS | ERA5 | JRA-55 | ERA5 | JRA-55 |
| 2006 | 51.1 | 51.3 | 55 | 347 | 364 | 361 | 366 |
| 2007 | 52.3 | 53.4 | 53.1 | 272 | 241 | 328 | 334 |
| 2008 | 54.5 | 54.6 | 56.5 | 296 | 319 | 355 | 362 |
| 2009 | 62.6 | 62.3 | 63.7 | 382 | 376 | 245 | 253 |
| 2010 | 56.1 | 56.2 | 59 | 285 | 258 | 209 | 218 |
| Mean | 55.3 | 55.6 | 57.5 | 316 | 312 | 299 | 307 |

(see Table 1). This melt become significant at the start of May and has a daily mean peak on 10 August of about 5 mm by both JRA-55 and ERA5-Land based simulations. The contribution of glacier melt begins to decline after August and becomes zero by the end of October. The analysis of monthly melt indicates that glacier melt contributes significantly in the river runoff from May to October with a peak in August. Simulations based on both data sets are well matched except the JRA-55 simulation showed comparatively slightly higher melt for May-June and ERA5-Land showed higher melt for July–September. The annual mean (Table 2) melt is 299 mm by ERA5-Land and 307 mm by JRA-55 for the 2006–2010 period. Maximum melt is simulated for 2006 at 361 mm and 366 mm while minimum is for 2010 at 209 mm and 218 mm by ERA5-Land and JRA-55 based simulations, respectively.

## 4.7. Discussion

### 4.7.1. Temperature

The temperature is a key input in hydrological modelling and one of the primary sources for analysing energy available for the melt process in high altitude river basins like Gilgit. However, due to an insufficient number of stations installed at higher altitudes and their non-uniform distribution, a temperature lapse rate is being used to derive temperature for higher elevation. Fixed values of lapse rate ranging from −5 to −8 °C km$^{-1}$ have been applied in UIB (Adnan et al., 2017; Tahir et al., 2011) and Qinghai Lake basin of north-eastern TP (Zhang et al., 2014). In this study, available temperature data from stations at different elevations are used to derive monthly lapse rates owing to the notable seasonal variation of temperature laps rates. We found that the method used to derive the temperature lapse rate (e.g. using annual, seasonal or monthly mean temperatures) makes a significant impact in a melt dominated catchment like the Gilgit. The TLR in the area is at its minimum in the post monsoon season and increases in September and reaches its highest in March. This minimum lapse rate observed for the post monsoon season may be associated with the strong heat exchange process during warm and moist atmospheric conditions (Kattel et al., 2013). Because of the monsoonal effect, moist adiabatic air motion is also frequent. This causes the release of latent heat due to water vapor condensation that increases the near-surface temperature at the higher elevations (Kattel et al., 2015). The winter/early spring records show the highest lapse rate values, potentially due to the weak heat exchange process during cool and dry atmospheric conditions (Barry and Chorley, 2009; Kattel et al., 2013). Moreover, with increase in the albedo effect of fresh snow cover during this season, cooling is strengthened at higher elevations.

### 4.7.2. Precipitation

The precipitation estimates appear more realistic and improved compared to gauged values from 1995 to 2010. The temporal precipitation distribution in the study area indicates that the basin receives significant precipitation in the form of snowfall during winter and spring seasons. This is similar to the findings of Tahir et al. (2016) who suggested that the runoff of the Gilgit Basin depends much more on snow and glacier melt than on rainfall. The distribution of precipitation in the study area indicates a very complex weather system due to local orographic effects and the multiple moisture sources including the winter westerlies and the Indian summer monsoon. Another possible reason may be that the study area is located just above the junction of three high mountain ranges the Hindukush, Himalaya and Karakorum. All these mountain ranges have different and diverse weather systems that ultimately generate very complex and mixed precipitation patterns in the Gilgit Basin. In addition, the basin is facing West Karakorum on its eastern part so the influence of the Karakorum based westerlies winter precipitation is evident from gauged data as well. There is one gauging station very close to the study area on the eastern side (Naltar; 2810 masl) in Karakorum Range. Those station data show an annual average precipitation of about 700 mm and most of it falls in winter/spring season in the form of snowfall. Winiger et al. (2005) have reported from 1991 to 96 data maximum annual snow depths of around 1200 and 1800 mm at Dame (3670 masl) and Diran (4050 masl) stations, respectively, in Bagrot Valley (Karakoram range), 20 km northeast of the Gilgit. They also reported that, along the Gilgit-Khunjerab transect within the Hunza basin, precipitation ranges between 600 and 1200 mm within the altitudes of 3500–4500 masl, of which 90% falls as snow.

The global data used in current study showed a slightly negative precipitation gradient in the study area. One possible reason for maximum precipitation in low elevation areas could be its wide elevation range (1454–2916 m) and presence of valleys bottoms in this range. Similar features of decreasing precipitation with increasing elevation was observed by Pang et al. (2014) in the central Himalayas where they concluded that precipitation above an elevation of 2400 masl decreases

significantly with increasing elevation. Hasson (2016) suggested that the reason Gilgit has low snow coverage at the higher elevation is that accumulated snow does not persist at high elevations due to the steep slopes. Dahri et al. (2016) concluded from their altitudinal analysis of precipitation distribution in HKH region that the typical orographic precipitation trend increases up to a certain height of maximum precipitation and thereafter decreases. This negative precipitation gradient is also evident from the station data. For instance, the Gupis station data showed the monthly mean precipitation in April as 62 mm while the higher altitude Yasin station data (3353 masl) showed this precipitation to be 45 mm for the same period. Similar features are evident between Gupis station (2198 masl) with a mean precipitation of 22.5 mm and Ushkore Station (3353 masl) with a mean precipitation of 21.5 mm for September. However, the number of stations is not sufficient and the scarcity of gauging stations discourages a development of a relationship between altitude and observed precipitation. Immerzeel et al. (2013) in their study in the Nepalese Himalayas, concluded that it is difficult to establish a uniform precipitation gradient due to the influence of several scale-dependent mechanisms. Dahri et al. (2016) also concluded that the complex altitudinal variation of precipitation in combination with highly diversified orography and multiple weather systems discourages the formulation of any single relation. Hence, the assumptions of linear increase in precipitation with elevation are not validated by this study.

### 4.7.3. Runoff

The evaluation of calibration and validation results shows that the DDD model performs reasonably well for poorly gauged basin. The model simulates flow and snowmelt based on a newly developed energy balance approach and glacier melt using degree day approach with global precipitation as input. The model showed a realistic quantitative estimate of melt contributions to the river flow. The main components of the river runoff of the study area include base flow, rainfall, snowmelt and glacial melt. The base flow is the low flow regime from October/November to March of next year. Base flow comes mainly from ground water, flow from lakes located in the study area and snowmelt at lower elevations during winter, where temperature rises above the melt threshold. The timings of peak flows in the observed and simulated hydrographs are different. This may be associated with the reason that these timings of peaks are largely determined by the input precipitation (rainfall/snowfall) and temperature than the parameters of the model. The model calibration is aimed at achieving the best model performance for the long-term daily discharge. Some improvements in the peak flows (magnitude and timing) may be gained if the calibration is targeted for peak flows only (e.g. if the purpose of the model is for flood forecasting), but even that would not be a lot effective for a long-term simulation. The global precipitation datasets have advantages particularly at the higher elevation areas where observation data are non-existent. Variability and extremes are of the major limitations of global data sets because of their low resolution and deficits for formulating the sub-grid developments (Kidd et al., 2013). So the sharp peaks generated by monsoon rainfalls may not be accurately simulated using global precipitation data sets. Another possible reason may be related to the spatial pattern of snow, which is also impacted by the limited availability of precipitation and temperature data. There are several other reasons associated with why very high skill scores are not achieved, including lack of gauged input data (precipitation and temperature in general), very sparse/no observations for cross validation of glacier melt and snow cover, very complex topography and local scale uncertainties.

### 4.7.4. SCA and SWE

Modelling a realistic status of snow, its spatial extent, variability, and contribution to river flow is important for understanding the hydrological regime of the study area. As mentioned previously, the observed temperature in the study area varies highly from a minimum

of −14 °C to a maximum of +16 °C and eventually influences all the temperature dependent processes such as SWE, SCA and glacial melt. The initial snowmelt starts at low elevations and extends to areas at higher elevation the temperature increases later in the summer. The snow accumulation starts in September and even earlier at higher altitudes and peaks in January/February when almost the entire study area (more than 90%) is covered with snow. Similar estimates of SCA were presented by (Hasson et al., 2014) who found the least SCA as 3 ± 1% during the summer season and maximum as 90 ± 4% during the spring season for the Gilgit Basin. Tahir et al. (2016) presented these estimates as varying between 12 and 85% for the Gilgit Basin based on 2000–2013 MODIS data. The RGI 6.0 data indicated that the study area has about 8.1% permanent glacier cover. This glacier is covered by snow in winter, but in the summer months, MODIS data may classify 8.1% of the area as snow when it really is glaciers. The DDD model keeps track of SCA and glaciers and this may be the reason why DDD has less SCA than in summer compared to MODIS.

The SWE estimates for the basin from 2006 to 2010 also seem quite reasonable. The DDD model shows SWE estimates for first time in the region. The snow pillows installed in the region by WAPDA faced transmission and rupture issues and made the SWE records limited to a very few stations. SWE measured at Deosai station (4149 masl) is between 400 and 700 mm from 2008 to 2013 (Hasson, 2016). These observations are higher that our simulated results, but these measurements are from the highly snowmelt dominated Astore Basin located in Himalayan Mountains and the station is located at high elevation while the DDD gives a catchment value.

### 4.7.5. Glacial melt

The simulation of glacier melt is carried out using a degree day approach. The glaciers are located in different elevation zones in the study area (derived from Randolph Glacier Inventory V 6.0) and their spatial coverage is used as input to the model. The model simulates the glacier melt on a daily basis from the study area. The melt simulations are in good agreement with the high flow regime of the river. Similar to snowmelt, the glacier melt also varies greatly with the variation in temperature. Fig. S5 shows variation in mean temperature of the basin versus variations in the glacier melt and possibly this is main reason behind this variation in glacier melt. The glacier melt timing is in good agreement with runoff and snowmelt timing of the study area. The snow starts melting in spring while glacier melt peaks in summer, but simulations showed there is an overlap of these melts (Fig. S6). One reason for this overlap is that the increase in temperature in early summer at low altitude can cause the glacier melts at the same time snow is still melting at higher altitudes. Another possibility for this overlapping melt from snow and glacier is that in glacier melt season, precipitation might fall as snow at higher altitude and then melt and contribute to the river runoff. A reverse characteristic is evident at the start of the accumulation season when snow starts to accumulate due to the decline in temperature in late summer at higher altitude and at the same time glaciers from comparatively lower altitude are still

melting. There might always be a mixed melt occurring in some part of the basin. Lutz et al. (2016) suggested a similar flow composition and mixed melt regimes for the Hunza basin in west Karakorum. Our findings suggest that separating these snow and glacier melt regimes based on the Julian day or the month as done by (Mukhopadhyay and Khan, 2015) does not apply in our study catchment.

### 4.8. Water balance

Water balance (WB) in a glaciated catchment can be represented as;

$$P + GM = Q + ET \pm \Delta S \qquad (4)$$

where, P is precipitation, GM is the contribution from glacier melt, Q is runoff, ET is the actual evapotranspiration and ΔS is the contribution from storages and soil moisture.

Water balance for the Gilgit Basin based on our simulations along with the mean percentages of inflow and outflow components is shown in Table 3. The inflow components include precipitation as rain, precipitation as snow, glaciers melt, and contribution from snow and subsurface storages and from soil moisture (ΔS). The outflow components include simulated flow and actual evapotranspiration. For the first year, ΔS is minus that means water is added to the soil and this is associated with the presence of snow from the previous year. Our results showed that precipitation as snow contributes more than precipitation as rain in the Gilgit Basin. Our simulations showed a mean annual contribution from rainfall of about 26%, snowmelt about 37–38%, glacier melt about 31% and storages and soil moisture about 5% to the river runoff. Mukhopadhyay and Khan (2015) analysed these contributions from monthly flow of the Gilgit River for two flow periods from 1966–1979 and 1980–2010. For the 1966–1979 period they estimated base flow (defined as flow due to precipitation as rain plus remnant melt) of about 32.5%, snowmelt of about 38%, and glacier melt of about 29.4%. For the 1980–2010 period they estimated base flow of about 32.1%, snowmelt of about 41.2%, and glacier melt of about 26.7%. In another paper Mukhopadhyay and Khan (2014a) from their monthly flow analysis for 1962–2010 period, estimated mean contributions from snowmelt of 38–43% and the glacier melt of 23–25%. However, their findings are based on flow regimes analysis and hydrograph separation using historical monthly flow data. Our estimates are based on daily scale modelling results where snow cover is simulated using an energy balance approach and glacier melt is simulated based on a degree day approach. Our simulation also showed an annual actual mean evapotranspiration of 202–221 mm (21–22% of total outflow). Bhutiyani (1999) estimated annual mean evaporation rates of 222 mm for Siachen glacier (eastern Karakoram) from 1986 to 1991. Reggiani and Rientjes (2015) estimated this as 200 ± 100 mm for the UIB from 1961 to 2009. Hence, our estimates of mean annual actual evapotranspiration also match well with the previous findings.

**Table 3**

Water balance of the Gilgit Basin using European reanalysis 5 (ERA5-Land) and Japanese reanalysis (JRA-55) precipitations as input to the model.

| Precipitation input | WB | WB/year | 2006 | 2007 | 2008 | 2009 | 2010 | Mean (mm) | Mean (%) |
|---|---|---|---|---|---|---|---|---|---|
| ERA5-Land | Inflow | Rain | 283 | 255 | 195 | 180 | 370 | 256 | 26.3 |
| | | Snow | 399 | 313 | 344 | 472 | 338 | 373 | 38.4 |
| | | GM | 361 | 328 | 355 | 245 | 209 | 299 | 30.8 |
| | | ΔS | −177 | 152 | 46 | 82 | 115 | 44 | 4.5 |
| | Outflow | Qsim | 656 | 836 | 713 | 798 | 849 | 770 | 79.2 |
| | | ET | 210 | 211 | 226 | 181 | 183 | 202 | 20.8 |
| JRA-55 | Inflow | Rain | 235 | 199 | 189 | 213 | 478 | 263 | 26.5 |
| | | Snow | 434 | 277 | 374 | 460 | 315 | 372 | 37.4 |
| | | GM | 366 | 334 | 362 | 253 | 218 | 307 | 30.9 |
| | | ΔS | −202 | 184 | 34 | 101 | 146 | 53 | 5.3 |
| | Outflow | Qsim | 597 | 753 | 712 | 831 | 970 | 773 | 77.8 |
| | | ET | 235 | 241 | 247 | 195 | 186 | 221 | 22.2 |

*4.9. Limitations of the study*

The study has a number of limitations associated with model structure and input data. Precipitation estimates are based on global precipitation products, which have certain limitations associated with spatial resolution, uncertainty, and limited ability to capture extremes. The proxy equations used in the energy balanced approach for snowmelt and evapotranspiration have shown reasonable results although the approach is coarse, i.e. neglecting spatial variability in topography, landscape types, temporal and spatial variability in wind speed and air pressure. The temperature data for all elevation zones in the basin were derived using lapse rates that are based on assumptions such as linear temperature increase with increasing elevation. The calibrated model parameters were not validated against any observed data from the study area. The model can potentially be improved applying parameters determined by field observation and by applying a finer scale land use cover.

## 5. Conclusions

Snow and glacier melt contributions to river runoff in the Gilgit Basin was analysed using a precipitation-runoff model. The precipitation-runoff model, Distance Distribution Dynamics (DDD), requires precipitation and temperature input data and is developed for snow dominated catchments in Norway. The precipitation input was derived from Global data sets (JRA-55 and ERA5-Land) and temperature input from station data using estimated lapse rates. The following conclusions can be drawn from this study:

- The precipitation estimates using global data sets for the Gilgit Basin showed quite promising results. The coarse grid size of the precipitation product does not necessarily translate into lower accuracy as the JRA-55 with 0.55° resolution performed comparably to ERA5-Land with 0.1° resolution. Most of the precipitation (68% by JRA-55 and 57% by ERA5-Land) in the study area falls as snow in the winter/spring season. A linear variation of precipitation with elevation cannot be applied for such high-altitude mountainous river basins with complex topography and multiple weather system. The runoff from the study area depends more on snowmelt (37–38%) and glacier melt (about 31%) than on the rainfall (26%). Realistic simulation of a variable for which the model is not calibrated against, such as SCA, gives confidence in the model structure and the realism of other simulated variables.

- The overlap in timing of melt from snow and glaciers (Fig. S6) indicates simultaneous melting for some time periods. The glaciers are located in different elevation zones in the study area with a higher fraction in higher altitude zones. The increasing temperature in early summer can melt simultaneously the glaciers at lower altitudes and snow at higher altitudes. Another reason for this overlapping melt is, during glacier melt season precipitation may fall as snow at higher altitudes melts and begins contributing to river runoff. In addition, snow does not melt completely, rather it keeps accumulating and melting throughout the year. The assumptions used in previous investigations, that snow is melting first completely before the glacial melt starts, are not supported by our results.

- The geographic information system in combination with remotely sensed data offer a great potential to understand and derive the runoff dynamics of the system. We found the DDD model reliable for data poor basins especially with a dominant snow or glacier melt component. Our modelling results provide a basis for future studies to simulate snow and glacier melt in surrounding basins with higher glacier cover. This can eventually facilitate more effective and sustainable downstream water resources management. However, more research in surrounding sub basins would help to strengthen and further substantiate current findings. The optimization of the model's parameters like liquid content in snow, threshold

temperature for snow/rain by in situ measurements from the region might further improve the results.

Supplementary data to this article can be found online at https://doi.org/10.1016/j.scitotenv.2021.149872.

## CRediT authorship contribution statement

Conception and design of study: A. Nazeer, S. Maskey, M. E. McClain.
Acquisition of data: A. Nazeer, S. Maskey, T. Skaugen.
Analysis and/or interpretation of data: A. Nazeer, S. Maskey, T. Skaugen, M. E. McClain.
Drafting the manuscript: A. Nazeer, S. Maskey, T. Skaugen, M. E. McClain.
Revising the manuscript critically for important intellectual content: A. Nazeer, S. Maskey, T. Skaugen, M. E. McClain.
Approval of the version of the manuscript to be published: A. Nazeer, S. Maskey, T. Skaugen, M. E. McClain.

## Declaration of competing interest

The authors declare that there is no conflict of interest.

## References

Adnan, M., Nabi, G., Kang, S., Zhang, G., Adnan, R.M., Anjum, M.N., Iqbal, M., Ali, A.F., 2017. Snowmelt runoff modelling under projected climate change patterns in the Gilgit River basin of northern Pakistan. Pol. J. Environ. Stud. 26 (3).

Akhtar, M., Ahmad, N., Booij, M.J., 2008. The impact of climate change on the water resources of Hindukush–Karakorum–Himalaya region under different glacier coverage scenarios. J. Hydrol. 355 (1–4), 148–163.

Andréassian, V., Perrin, C., Michel, C., Usart-Sanchez, I., Lavabre, J., 2001. Impact of imperfect rainfall knowledge on the efficiency and the parameters of watershed models. J. Hydrol. 250 (1–4), 206–223.

Archer, D.R., Fowler, H.J., 2004. Spatial and temporal variations in precipitation in the upper Indus Basin, global teleconnections and hydrological implications. Hydrol. Earth Syst. Sci. 8, 47–61.

Barnett, T.P., Adam, J.C., Lettenmaier, D.P., 2005. Potential impacts of a warming climate on water availability in snow-dominated regions. Nature 438 (7066), 303–309.

Barry, R.G., Chorley, R.J., 2009. Atmosphere, Weather and Climate. Routledge.

Berthier, E., Arnaud, Y., Vincent, C., Remy, F., 2006. Biases of SRTM in high-mountain areas: implications for the monitoring of glacier volume changes. Geophys. Res. Lett. 33 (8).

Bhutiyani, M., 1999. Mass-balance studies on Siachen glacier in the Nubra valley, Karakoram Himalaya, India. J. Glaciol. 45 (149), 112–118.

Bocchiola, D., Diolaiuti, G., Soncini, A., Mihalcea, C., D'Agata, C., Mayer, C., Lambrecht, A., Rosso, R., Smiraglia, C., 2011. Prediction of future hydrological regimes in poorly gauged high altitude basins: the case study of the upper Indus, Pakistan. Hydrol. Earth Syst. Sci. 15 (7), 2059–2075.

Bookhagen, B., Burbank, D.W., 2006. Topography, relief, and TRMM-derived rainfall variations along the Himalaya. Geophys. Res. Lett. 33 (8).

Cannon, F., Carvalho, L.M., Jones, C., Bookhagen, B., 2015. Multi-annual variations in winter westerly disturbance activity affecting the Himalaya. Clim. Dyn. 44 (1–2), 441–455.

Cramer, W.P., Leemans, R., 1993. Vegetation Dynamics & Global Change. Springer, pp. 190–217.

Dahri, Z.H., Ludwig, F., Moors, E., Ahmad, B., Khan, A., Kabat, P., 2016. An appraisal of precipitation distribution in the high-altitude catchments of the indus basin. Sci. Total Environ. 548, 289–306.

Dahri, Z.H., Ludwig, F., Moors, E., Ahmad, S., Ahmad, B., Ahmad, S., Riaz, M., Kabat, P., 2021. Climate change and hydrological regime of the high-altitude indus basin under extreme climate scenarios. Sci. Total Environ. 768, 144467.

Essery, R., Morin, S., Lejeune, Y., Ménard, C.B., 2013. A comparison of 1701 snow models using observations from an alpine site. Adv. Water Resour. 55, 131–148.

Gupta, H.V., Kling, H., Yilmaz, K.K., Martinez, G.F., 2009. Decomposition of the mean squared error and NSE performance criteria: implications for improving hydrological modelling. J. Hydrol. 377 (1–2), 80–91.

Hasson, S.U., 2016. Future water availability from Hindukush-Karakoram-Himalaya upper Indus Basin under conflicting climate change scenarios. Climate 4 (4).

Hasson, S., Lucarini, V., Khan, M.R., Petitta, M., Bolch, T., Gioli, G., 2014. Early 21st century snow cover state over the western river basins of the Indus River system. Hydrol. Earth Syst. Sci. 18 (10), 4077–4100.

Herold, N., Behrangi, A., Alexander, L.V., 2017. Large uncertainties in observed daily precipitation extremes over land. J. Geophys. Res. Atmos. 122 (2), 668–681.

Hussan, W.U., Khurram Shahzad, M., Seidel, F., Nestmann, F., 2020. Application of soft computing models with input vectors of snow cover area in addition to hydroclimatic data to predict the sediment loads. Water 12 (5), 1481.

Immerzeel, W.W., Pellicciotti, F., Shrestha, A.B., 2012. Glaciers as a proxy to quantify the spatial distribution of precipitation in the Hunza Basin. Mt. Res. Dev. 32 (1), 30–38.

Immerzeel, W.W., Pellicciotti, F., Bierkens, M.F.P., 2013. Rising river flows throughout the twenty-first century in two Himalayan glacierized watersheds. Nat. Geosci. 6 (9), 742–745.

Immerzeel, W.W., Wanders, N., Lutz, A.F., Shea, J.M., Bierkens, M.F.P., 2015. Reconciling high-altitude precipitation in the upper indus basin with glacier mass balances and runoff. Hydrol. Earth Syst. Sci. 19 (11), 4673–4687.

Kaab, A., Berthier, E., Nuth, C., Gardelle, J., Arnaud, Y., 2012. Contrasting patterns of early twenty-first-century glacier mass change in the Himalayas. Nature 488 (7412), 495–498.

Kapnick, S.B., Delworth, T.L., Ashfaq, M., Malyshev, S., Milly, P.C., 2014. Snowfall less sensitive to warming in Karakoram than in Himalayas due to a unique seasonal cycle. Nat. Geosci. 7 (11), 834–840.

Kattel, D., Yao, T., Yang, K., Tian, L., Yang, G., Joswiak, D., 2013. Temperature lapse rate in complex mountain terrain on the southern slope of the Central Himalayas. Theor. Appl. Climatol. 113 (3–4), 671–682.

Kattel, D.B., Yao, T., Yang, W., Gao, Y., Tian, L., 2015. Comparison of temperature lapse rates from the northern to the southern slopes of the Himalayas. Int. J. Climatol. 35 (15), 4431–4443.

Khan, A., Richards, K.S., Parker, G.T., McRobie, A., Mukhopadhyay, B., 2014. How large is the upper Indus Basin? The pitfalls of auto-delineation using DEMs. J. Hydrol. 509, 442–453.

Kidd, C., Dawkins, E., Huffman, G., 2013. Comparison of precipitation derived from the ECMWF operational forecast model and satellite precipitation datasets. J. Hydrometeorol. 14 (5), 1463–1482.

Knoben, W.J., Freer, J.E., Woods, R.A., 2019. Inherent benchmark or not? Comparing Nash-sutcliffe and kling-gupta efficiency scores. Hydrol. Earth Syst. Sci. 23 (10), 4323–4331.

Kobayashi, S., Ota, Y., Harada, Y., Ebita, A., Moriya, M., Onoda, H., Onogi, K., Kamahori, H., Kobayashi, C., Endo, H., 2015. The JRA-55 reanalysis: general specifications and basic characteristics. J. Meteorol. Soc. Jpn. Ser. II 93 (1), 5–48.

Krasovskaia, I., Arnell, N., Gottschalk, L., 1994. Flow regimes in northern and western Europe: development and application of procedures for classifying flow regimes. IAHS Publications-Series of Proceedings and Reports-Intern Assoc Hydrological Sciences. 221, pp. 185–192.

Latif, Y., Ma, Y., Ma, W., Muhammad, S., Adnan, M., Yaseen, M., Fealy, R., 2020. Differentiating snow and glacier melt contribution to runoff in the Gilgit River basin via degree-day modelling approach. Atmosphere 11 (10), 1023.

Lutz, A., Immerzeel, W., Shrestha, A., Bierkens, M., 2014a. Consistent increase in high Asia's runoff due to increasing glacier melt and precipitation. Nat. Clim. Chang. 4 (7), 587–592.

Lutz, A.F., Immerzeel, W.W., Kraaijenbrink, P.D., Shrestha, A.B., Bierkens, M.F., 2016. Climate change impacts on the upper indus hydrology: sources, shifts and extremes. PLoS One 11 (11), e0165630.

Martens, B., Cabus, P., De Jongh, I., Verhoest, N., 2013. Merging weather radar observations with ground-based measurements of rainfall using an adaptive multiquadric surface fitting algorithm. J. Hydrol. 500, 84–96.

Michaelides, S., Levizzani, V., Anagnostou, E., Bauer, P., Kasparis, T., Lane, J., 2009. Precipitation: measurement, remote sensing, climatology and modeling. Atmos. Res. 94 (4), 512–533.

Minora, U., Bocchiola, D., D'Agata, C., Maragno, D., Mayer, C., Lambrecht, A., Vuillermoz, E., Senese, A., Compostella, C., Smiraglia, C., Diolaiuti, G.A., 2016. Glacier area stability in the Central Karakoram National Park (Pakistan) in 2001–2010. Prog. Phys. Geogr. 40 (5), 629–660.

Mugnai, A., Casella, D., Cattani, E., Dietrich, S., Laviola, S., Levizzani, V., Panegrossi, G., Petracca, M., Sanò, P., Paola, F.D., 2013. Precipitation products from the hydrology SAF. Nat. Hazards Earth Syst. Sci. 13 (8), 1959–1981.

Muhammad, S., Tian, L., Khan, A., 2019. Early twenty-first century glacier mass losses in the Indus Basin constrained by density assumptions. J. Hydrol. 574, 467–475.

Mukhopadhyay, B., Khan, A., 2014a. A quantitative assessment of the genetic sources of the hydrologic flow regimes in upper Indus Basin and its significance in a changing climate. J. Hydrol. 509, 549–572.

Mukhopadhyay, B., Khan, A., 2014b. Rising river flows and glacial mass balance in Central Karakoram. J. Hydrol. 513, 192–203.

Mukhopadhyay, B., Khan, A., 2015. A reevaluation of the snowmelt and glacial melt in river flows within upper Indus Basin and its significance in a changing climate. J. Hydrol. 527, 119–132.

Muñoz Sabater, J., 2019. ERA5-Land monthly averaged data from 1981 to present. Copernicus Climate Change Service (C3S) Climate Data Store (CDS).

Pang, H., Hou, S., Kaspari, S., Mayewski, P., 2014. Influence of regional precipitation patterns on stable isotopes in ice cores from the Central Himalayas. Cryosphere 8 (1), 289.

Prasad, V.H., Roy, P.S., 2005. Estimation of snowmelt runoff in Beas Basin, India. Geocarto Int. 20 (2), 41–47.

Reggiani, P., Rientjes, T., 2015. A reflection on the long-term water balance of the upper Indus Basin. Hydrol. Res. 46 (3), 446–462.

Schaner, N., Voisin, N., Nijssen, B., Lettenmaier, D.P., 2012. The contribution of glacier melt to streamflow. Environ. Res. Lett. 7 (3), 034029.

Shafeeque, M., Luo, Y., Wang, X., Sun, L., 2019. Revealing vertical distribution of precipitation in the glacierized upper Indus Basin based on multiple datasets. J. Hydrometeorol. 20 (12), 2291–2314.

Sharif, M., Archer, D.R., Fowler, H.J., Forsythe, N., 2013. Trends in timing and magnitude of flow in the upper Indus Basin. Hydrol. Earth Syst. Sci. 17 (4), 1503–1516.

SIHP: Snow and Ice Hydrology, 1997. Phase-II Final Report to CIDA. International Development Research Centre, Ottawa, Ontario, Canada.

Skaugen, T., Mengistu, Z., 2016. Estimating catchment-scale groundwater dynamics from recession analysis &ndash; enhanced constraining of hydrological models. Hydrol. Earth Syst. Sci. 20 (12), 4963–4981.

Skaugen, T., Onof, C., 2014. A rainfall-runoff model parameterized from GIS and runoff data. Hydrol. Process. 28 (15), 4529–4542.

Skaugen, T., Saloranta, T., 2015. Simplified Energy-balance Snowmelt Modelling. NVE Report 31.

Skaugen, T., Weltzien, I.H., 2016. A model for the spatial distribution of snow water equivalent parameterized from the spatial variability of precipitation. Cryosphere 10 (5), 1947–1963.

Skaugen, T., Luijting, H., Saloranta, T., Vikhamar-Schuler, D., Müller, K., 2018. In search of operational snow model structures for the future – comparing four snow models for 17 catchments in Norway. Hydrol. Res. 49 (6), 1929–1945.

Smith, R.B., 2006. Progress on the theory of orographic precipitation. Geol. Soc. Am. Spec. Pap. 398, 1.

Tahir, A.A., Chevallier, P., Arnaud, Y., Neppel, L., Ahmad, B., 2011. Modeling snowmelt-runoff under climate scenarios in the Hunza River basin, Karakoram range, northern Pakistan. J. Hydrol. 409 (1–2), 104–117.

Tahir, A.A., Adamowski, J.F., Chevallier, P., Haq, A.U., Terzago, S., 2016. Comparative assessment of spatiotemporal snow cover changes and hydrological behavior of the gilgit, astore and Hunza River basins (Hindukush–Karakoram–Himalaya region, Pakistan). Meteorog. Atmos. Phys. 128 (6), 793–811.

Tekeli, A.E., Akyürek, Z., Arda Sorman, A., Sensoy, A., Ünal Sorman, A., 2005. Using MODIS snow cover maps in modeling snowmelt runoff process in the eastern part of Turkey. Remote Sens. Environ. 97 (2), 216–230.

Tong, X., Shi, W., Deng, S., 2009. A probability-based multi-measure feature matching method in map conflation. Int. J. Remote Sens. 30 (20), 5453–5472.

Walter, M.T., Brooks, E.S., McCool, D.K., King, L.G., Molnau, M., Boll, J., 2005. Process-based snowmelt modeling: does it require more input data than temperature-index modeling? J. Hydrol. 300 (1–4), 65–75.

Winiger, M., Gumpert, M., Yamout, H., 2005. Karakorum–Hindukush–western Himalaya: assessing high-altitude water resources. Hydrol. Process. 19 (12), 2329–2338.

Zhang, G., Xie, H., Yao, T., Li, H., Duan, S., 2014. Quantitative water resources assessment of Qinghai Lake basin using snowmelt runoff model (SRM). J. Hydrol. 519, 976–987.